2008 IEEE International Conference on
Robotics and Automation
Pasadena, CA, USA, May 19-23, 2008

Planning of Smooth Motions for a Ball-Plate System With Limited Contact Area

Mikhail Svinin and Shigeyuki Hosoe

Abstract— **The paper deals with the motion planning for a rolling system with limited contact area. The system under consideration is represented by a hemispherical object that can roll without slipping or spinning on the plane. Under the constraints imposed on the size of the contact area, the construction of motion can be regarded as a problem of parallel parking in a finite number of movement steps. A motion planning algorithm, realizing the movement steps by tracing smooth figure eights on the hemisphere, is introduced. To generate asymmetric figure eights, a generalization of the Viviani curve is proposed. An exceptional case of the algorithm, corresponding to a spinning maneuver, is constructed with the use of the Cassini curve. The convergence of the algorithm is analyzed and its computational feasibility is verified under simulation.**

I. Introduction

One of the key problems in the control of systems with rolling constraints is the construction of motion planning algorithms. In this paper we address this problem in the kinematic formulation. We will be dealing with a typical example of systems with pure rolling constraints, the ball-plate system. It is known that this system is controllable [1]. However, it is neither nilpotent nor differentially flat, and therefore it cannot be put in chained form [2]. These features set the ball-plate system into a special class of non-holonomic systems, the class for which conventional planning techniques are not applicable.

One can divide the existing approaches to motion planning for the ball-plate system into two directions depending on whether they are constructed in feedforward or feedback [3]–[6] manner. The feedforward motion planning algorithms can be, in turn, classified into two approaches. The first is based on the optimal control theory [7]–[9], while the second deals with geometric phases [1], [10], [11]. The geometric phase approach is based on the fact that a closed path of the control inputs results in a change of the contact coordinates. For the ball-plate system it was first outlined in [1], where a three-step algorithm combining one trivial and two non-trivial maneuvers was proposed. This approach was revisited in [12], where the number of non-trivial maneuvers was reduced to one. A more general algorithm, based on the transformation of the state equations of the kinematic model to a triangular form and the use of alternating piecewise constant inputs, was proposed in [13]. As shown there, the triangular form allows to reduce the motion planning problem to solving a system of two nonlinear algebraic equations.

M. Svinin and S. Hosoe are with Bio-Mimetic Control Research Center, RIKEN, Anagahora, Shimoshidami, Moriyama-ku, Nagoya, Aichi 463-0003, Japan svinin(hosoe)@bmc.riken.jp

It should be noted that most of the algorithms proposed so far are devised for the whole sphere case. However, in a number of applications the rolling motion must be conducted under constraints imposed on the size of the contact area. One of the first studies addressing the motion planning under such constraints is reported in [14]. The motion planning algorithm proposed in [14] utilizes the main ideas of [1] and is based on the construction of a set of multiple spherical triangles on the object surfaces. Also relevant to our research is the study [15], where a motion planning algorithm, possessing a local-local topological property [16], was proposed. The non-trivial maneuver of the planning algorithm in [15] is composed of geodesic quadrilaterals whose size depends on the workspace limitations. A somewhat similar algorithm, iterating trapezoidal paths on the sphere, was proposed in [17].

It should be noted that employing spherical polygons is not always the best way to plan the rolling motion, especially if the speed of the whole maneuver needs to be taken into consideration. The algorithms [14], [15], [17] produce piecewise smooth trajectories, but the motion of the system needs to be stopped at the vertices of the spherical polygons if one cares about generating impact-free movements. In this connection, it can be more advantageous to replace the polygons by smoother curves. In the simplest formulation, the motion strategy can be based on tracing smooth figure eights on the spherical object.

As shown in [18], the composition of figure eights from two circles does not produce C^∞ trajectories, and the switching point between the two circles needs to be passed with zero instantaneous velocity. To generate infinitely smooth trajectories, a generalization of the Viviani curve was proposed in [18]. However, the generalization used in [18] is not always well-defined and in some cases it produces curves with three petals. To improve upon this shortcoming, in this paper we propose a rigorous and at the same time geometrically clear way to construct asymmetric figure eights and define the reachability area for the parameterization obtained. In addition, we show how the motion strategy based on tracing smooth figure eights can be modified to realize a spinning maneuver.

This paper is organized as follows. In Section II we sketch a model of the ball-plate system and fix the notation. A motion planning algorithm, based on tracing smooth figure eights, is introduced in Section III. To generate C^∞ trajectories, in Section IV we derive a generalized Viviani curve and test the performance of the motion planning algorithm under simulation. Section V addresses the exceptional case of the algorithm, corresponding to a spinning maneuver. Finally,

978-1-4244-1647-9/08/$25.00 ©2008 IEEE.

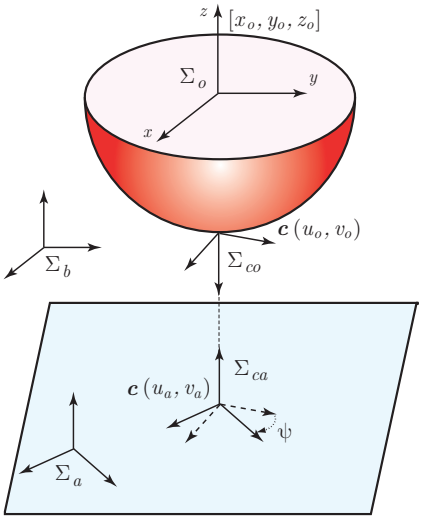

Fig. 1. System formalization.

conclusions are summarized in Section VI.

II. Mathematical Model

To describe the system under consideration, we introduce the following coordinate frames (see Figure 1): Σ_b is an inertial frame fixed at the base, Σ_o is a frame fixed at the geometric center of the object (hemisphere), Σ_a is a frame fixed at the contact plane. In addition, at the contact point we introduce the contact frame of the object Σ_{co}, and the contact frame of the plane, Σ_{ca}.

The contact coordinates are given by the vectors $\boldsymbol{u}_{co} = [u_o, v_o]^{\mathrm{T}}$, expressing the contact point on the hemisphere surface, $\boldsymbol{u}_{ca} = [u_a, v_a]^{\mathrm{T}}$, expressing the contact point on the plane, and by the contact angle ψ which is defined as the angle between the x-axis of Σ_{co} and Σ_{ca}. The position of a point on the sphere is parameterized as

$$\boldsymbol{c}(u_o, v_o) = R \begin{bmatrix} -\sin u_o \cos v_o \\ \sin v_o \\ -\cos u_o \cos v_o \end{bmatrix}, \tag{1}$$

where R is the radius of the sphere. In this parameterization the origin is placed at the south pole of the sphere. The lower hemisphere is selected by imposing

$$-\pi/2 < u_o < \pi/2, \quad -\pi/2 < v_o < \pi/2. \tag{2}$$

The machinery of the derivation of the contact kinematic equations under the assumption of pure rolling can be found in [11]. For the parameterization (1) we obtain:

$$\begin{aligned} \dot{u}_o &= \sec v_o(-\cos\psi\,\dot{u}_a + \sin\psi\,\dot{v}_a)/R, && (3)\\ \dot{v}_o &= (\sin\psi\,\dot{u}_a + \cos\psi\,\dot{v}_a)/R, && (4)\\ \dot{\psi} &= \tan v_o(-\cos\psi\,\dot{u}_a + \sin\psi\,\dot{v}_a)/R. && (5) \end{aligned}$$

If the position of the contact point in the contact plane is parameterized as $\boldsymbol{u}_{ca} = \boldsymbol{u}_{ca}(\varphi)$ from (3-5) we obtain the system

$$\begin{aligned} u_o'(\varphi) &= \sec v_o(\varphi)(\sin\psi(\varphi)v_a'(\varphi) - \cos\psi(\varphi)u_a'(\varphi))/R, && (6)\\ v_o'(\varphi) &= (\sin\psi(\varphi)u_a'(\varphi) + \cos\psi(\varphi)v_a'(\varphi))/R, && (7)\\ \psi'(\varphi) &= \tan v_o(\varphi)(\sin\psi(\varphi)v_a'(\varphi) - \cos\psi(\varphi)u_a'(\varphi))/R, && (8) \end{aligned}$$

describing the change of the contact coordinates as function of φ. Here, primes denote the partial differentiation with respect to the variable φ, while dots are reserved for the time differentiation.

The kinematic model (3-5) can be represented in a different form if the input variables are the components of $\dot{\boldsymbol{u}}_{co}$. This form is given as

$$\begin{aligned} \dot{u}_a &= -R\cos\psi\cos v_o\,\dot{u}_o + R\sin\psi\,\dot{v}_o, && (9)\\ \dot{v}_a &= R\sin\psi\cos v_o\,\dot{u}_o + R\cos\psi\,\dot{v}_o, && (10)\\ \dot{\psi} &= \sin v_o\,\dot{u}_o. && (11) \end{aligned}$$

Assume that the position of the contact point on the sphere is parameterized by a spherical curve $\boldsymbol{c}(\varphi) \triangleq \{x(\varphi), y(\varphi), z(\varphi)\}^{\mathrm{T}}$. Since the same point is defined by (1), one has

$$\boldsymbol{c}(u_o, v_o) = \boldsymbol{c}(\varphi). \tag{12}$$

Differentiating this relationship, one obtains

$$\boldsymbol{c}_u\dot{u}_o + \boldsymbol{c}_v\dot{v}_o = \boldsymbol{c}_\varphi\dot{\varphi}, \tag{13}$$

where $\boldsymbol{c}_\varphi \triangleq \partial\boldsymbol{c}/\partial\varphi$, $\boldsymbol{c}_u \triangleq \partial\boldsymbol{c}/\partial u_o$ and $\boldsymbol{c}_v \triangleq \partial\boldsymbol{c}/\partial v_o$. The partial derivatives $\boldsymbol{c}_u$ and $\boldsymbol{c}_v$,

$$\boldsymbol{c}_u = R\begin{bmatrix} -\cos u_o\cos v_o \\ 0 \\ \sin u_o\cos v_o \end{bmatrix}, \quad \boldsymbol{c}_v = R\begin{bmatrix} \sin u_o\sin v_o \\ \cos v_o \\ \cos u_o\sin v_o \end{bmatrix}, \tag{14}$$

are defined from (1). To express $\boldsymbol{c}_u$ and $\boldsymbol{c}_v$ as functions of φ, one resolves (12) and obtains

$$\begin{aligned} \cos v_o &= \sqrt{1-(y(\varphi)/R)^2}, \ \ \sin v_o = y(\varphi)/R, && (15)\\ \cos u_o &= \frac{-z(\varphi)/R}{\sqrt{1-(y(\varphi)/R)^2}}, \ \ \sin u_o = \frac{-x(\varphi)/R}{\sqrt{1-(y(\varphi)/R)^2}}, && (16) \end{aligned}$$

Therefore,

$$\boldsymbol{c}_u = \begin{bmatrix} z(\varphi) \\ 0 \\ -x(\varphi) \end{bmatrix}, \ \boldsymbol{c}_v = \begin{bmatrix} -x(\varphi)y(\varphi)/\sqrt{R^2-y^2(\varphi)} \\ \sqrt{R^2-y^2(\varphi)} \\ -y(\varphi)z(\varphi)/\sqrt{R^2-y^2(\varphi)} \end{bmatrix}, \tag{17}$$

Next, taking into account that the vectors $\boldsymbol{c}_u$ and $\boldsymbol{c}_v$ are orthogonal, one obtains from (13)

$$\dot{u}_o = \frac{1}{R^2\cos^2 v_o}\boldsymbol{c}_u^{\mathrm{T}}\boldsymbol{c}_\varphi\dot{\varphi}, \quad \dot{v}_o = \frac{1}{R^2}\boldsymbol{c}_v^{\mathrm{T}}\boldsymbol{c}_\varphi\dot{\varphi}, \tag{18}$$

and substituting (18) into (9-11) yields

$$\begin{aligned} u_a'(\varphi) &= -\frac{\cos\psi(\varphi)}{\sqrt{R^2-y^2(\varphi)}}\boldsymbol{c}_u^{\mathrm{T}}\boldsymbol{c}_\varphi + \frac{\sin\psi(\varphi)}{R}\boldsymbol{c}_v^{\mathrm{T}}\boldsymbol{c}_\varphi, && (19)\\ v_a'(\varphi) &= \frac{\sin\psi(\varphi)}{\sqrt{R^2-y^2(\varphi)}}\boldsymbol{c}_u^{\mathrm{T}}\boldsymbol{c}_\varphi + \frac{\cos\psi(\varphi)}{R}\boldsymbol{c}_v^{\mathrm{T}}\boldsymbol{c}_\varphi, && (20)\\ \psi'(\varphi) &= \frac{y(\varphi)}{R(R^2-y^2(\varphi))}\boldsymbol{c}_u^{\mathrm{T}}\boldsymbol{c}_\varphi. && (21) \end{aligned}$$

III. Motion Planning Strategy

In this section we address the motion planning problem (state-to-state transfer) under the assumption that at the start and end configurations the initial and final values of $\boldsymbol{u}_{co}$ are zero. The assumption restricts the generality of the problem statement. However, the movement to be found under this assumption can be thought of as a non-trivial maneuver of a general reconfiguration strategy similar to that considered in [1], [12], [13]. The generality can be restored if the non-trivial maneuver is accompanied by a trivial one (bringing $\boldsymbol{u}_{co}$ to the desired values). As the change of the contact coordinates $\boldsymbol{u}_{ca}$ and ψ corresponding to the trivial maneuver can be computed in advance, their desired values can be simply modified, and the trivial maneuver can be executed right after the non-trivial one.

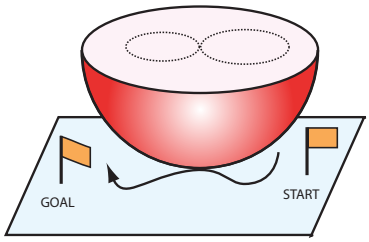

Fig. 2. Motion planning problem. Dotted lines show the projection of the contact point on the hemisphere onto the main hemisphere plain.

To take into consideration the constraints on the size of the contact area, we will restrict the height of the admissible spherical cap. Since the full-scale rolling is now impossible, a feasible motion planning strategy can be based on tracing closed curves on the surface of the sphere n times. Tracing the curve one time can be called a movement step. Thus, the non-trivial maneuver considered in the section can be regarded, in general, as a hybrid parallel parking problem (see Figure 2). It is hybrid because in addition to continuous variables (contact coordinates) it includes the discrete number of movement steps.

To generate smooth trajectories for the non-trivial maneuver, one can parameterize the position of the contact point on the sphere by a single periodic curve $\boldsymbol{c}(\varphi) = \boldsymbol{c}(\varphi \pm 2k\pi)$, $k \in \mathbb{Z}$, such that $\boldsymbol{c}(0) = \{0, 0, -R\}^{\mathrm{T}}$ and therefore $u_o(2\pi n) = v_o(2\pi n) = 0$. To satisfy the remaining boundary conditions $u_a(2\pi n) = u_{a,\mathrm{des}}$, $v_a(2\pi n) = v_{a,\mathrm{des}}$, $\psi(2\pi n) = \psi_{\mathrm{des}}$, for a given the number of steps n, there must be at least three free parameters in a specific representation of the curve $\boldsymbol{c}(\varphi)$.

In what follows, we will define $\boldsymbol{c}(\varphi)$ by asymmetric spherical figure eights. Conceptually, the motion planning problem can be then formulated as follows. Given a smooth spherical figure eight, find its initial orientation on the sphere, given by the angle ϑ of rotation around the axis OZ of the frame Σ_o, and the sizes a and b of its two leaves such that tracing the curve n times brings the system to the desired configuration. More specifically, we define

$$\boldsymbol{c}(\varphi) = \boldsymbol{R}_z(\vartheta)\bar{\boldsymbol{c}}(a, b, \varphi), \tag{22}$$

where

$$\boldsymbol{R}_z(\vartheta) \triangleq \begin{bmatrix} \cos\vartheta & -\sin\vartheta & 0 \\ \sin\vartheta & \cos\vartheta & 0 \\ 0 & 0 & 1 \end{bmatrix}, \tag{23}$$

and reduce the motion planning problem to finding the parameters a, b, and ϑ. Computationally, the motion planning procedure can be decoupled into two stages. At the first stage we define the generalized parameters a and b, and at the second stage we define the angle ϑ.

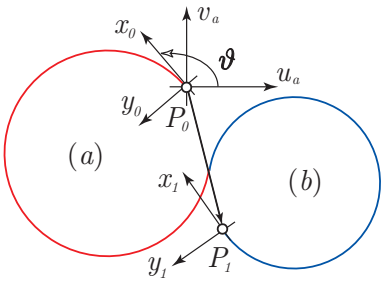

Fig. 3. One-step movement in the contact plane. The 1st half-step (tracing the 1st leaf of the figure eight) is shown in red, while the 2nd in blue color. Also shown are the initial orientation and the assignment of local frames.

If we trace the spherical figure eight one time, the contact point in the contact plane is shifted from P_0 to P_1 as shown schematically in Figure 3. We will call the length of the linear displacement $h = |\overrightarrow{P_0P_1}|$ the non-holonomic shift. In Figure 3 we also introduce local frames associated with the movement steps. It is assumed that the x-axes of the local frames are oriented along the tangent vectors to the contact curve in the contact plane. The orientation of the frame $P_1x_1y_1$ with respect to $P_0x_0y_0$ defines the holonomy angle η. Note that the angle ϑ, defining the orientation of the frame $P_0x_0y_0$ with respect to the frame Σ_a is unknown at the moment. It will be adjusted later on from the requirement that the vector of the resulting displacement should point to the desired destination.

It is clear that the non-holonomic shift h and the holonomy angle η are the same for all the movement steps. They are functions of the generalized parameters a and b and do not depend on the angle ϑ. To compute $h(a, b)$ and $\eta(a, b)$, we set in (22) $\vartheta = 0$ and integrate the system (19-21) numerically for one step of movement ($\varphi \in [0, 2\pi]$) with zero initial conditions. This defines $h(a, b) \triangleq \sqrt{\bar{u}_a^2(2\pi) + \bar{v}_a^2(2\pi)}$ and $\eta(a, b) \triangleq \bar{\psi}(2\pi)$. Here, we use the bar to denote the contact coordinates obtained for $\vartheta = 0$.

Having formally defined the functions $h(a, b)$ and $\eta(a, b)$, we establish their relation with $h_{\mathrm{des}} = \sqrt{u_{a,\mathrm{des}}^2 + v_{a,\mathrm{des}}^2}$ and ψ_{des}. As we trace the spherical figure eight n times, the vector of the non-holonomic shift will rotate each time by the angle η as shown in Figure 4. Therefore, the points $P_0, P_1, \ldots, P_n$ will lie on a circle of (now unknown) radius r and form a part of what may appear to be a regular polygon[1]. Clearly,

$$\eta(a, b) = \psi_{\mathrm{des}}/n. \tag{24}$$

[1]In fact, the points will be a part of a regular polygon only if the ratio $2\pi n/\psi_{\mathrm{des}}$ is integer.

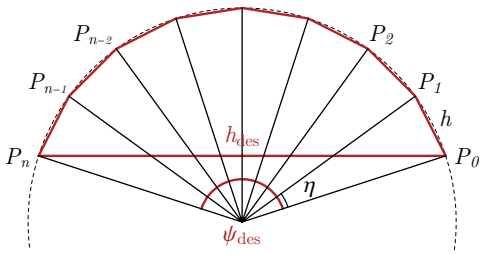

Fig. 4. The change of the vectors of the non-holonomic shift during n-step movement.

The formula for $h(a,b)$ can also be found from elementary considerations. Indeed, from the relation between the length of the chord of a circular arc and the corresponding central angle we have

$$h(a,b) = 2r\sin(\eta(a,b)/2), \tag{25}$$

and

$$h_{\text{des}} = 2r\sin(n\,\eta(a,b)/2), \tag{26}$$

where r is the radius of the circular arc. Excluding it from equations (25,26), we obtain

$$h(a,b) = \frac{\sin(\eta(a,b)/2)}{\sin(n\,\eta(a,b)/2)}h_{\text{des}} = \frac{\sin(\psi_{\text{des}}/2n)}{\sin(\psi_{\text{des}}/2)}h_{\text{des}}. \tag{27}$$

Now, one can determine the parameters a and b from solving the system (24,27). The practical calculation the parameters a and b may seem to be involved because these parameters are obtained by iterating the nonlinear system (24,27) with numerical integration of the system (19-21) on each iteration step. However, in our experience this procedure is computationally feasible. With a good guess on the initial values of a and b the solution is obtained relatively fast, within a few seconds in our software implementation. The computational feasibility is attributed by the low dimension and the regular structure of the system (19-21).

Having established a and b, one can define the angle ϑ. The total linear displacement during n-step movement is defined in the vectorial form as $\boldsymbol{d} = \sum_{k=0}^{n-1}\overrightarrow{P_kP_{k+1}}$. The projection of the vector $\boldsymbol{d}$ onto the axes of Σ_a and onto the axes of the frame $P_0x_0y_o$ are denoted as, respectively, $\boldsymbol{d}^{(a)}$ and $\boldsymbol{d}^{(0)}$. They are related as

$$\boldsymbol{d}^{(a)} = R_z(\vartheta)\boldsymbol{d}^{(0)}, \tag{28}$$

where the matrix $R_z(\vartheta)$ is the upper diagonal 2×2 block of the matrix (23). By definition, $\boldsymbol{d}^{(a)} = \{u_{a,\text{des}}, v_{a,\text{des}}\}^{\text{T}}$. Since the mutual orientation of two adjacent local frames, associated with the multi-step movement, is defined by the angle $\eta(a,b)$, expressing the vector $\boldsymbol{d}$ in the axes of $P_0x_0y_o$ yields

$$\boldsymbol{d}^{(0)} = \sum_{k=0}^{n-1} R_z^k(\eta(a,b))\overrightarrow{P_0P_1}^{(0)}, \tag{29}$$

where the vector $\overrightarrow{P_0P_1}^{(0)} = \{\bar{u}_a(2\pi), \bar{v}_a(2\pi)\}^{\text{T}}$ was defined at the first stage of the algorithm. Having defined $\boldsymbol{d}^{(a)}$ and $\boldsymbol{d}^{(0)}$, we can calculate the angle between these vectors. Taking into account that $|\boldsymbol{d}^{(a)}| = |\boldsymbol{d}^{(a)}| = h_{\text{des}}$, one obtains

$$\vartheta = \arccos\frac{\boldsymbol{d}^{(0)}\cdot\boldsymbol{d}^{(a)}}{h_{\text{des}}^2}. \tag{30}$$

This completes the description of the motion planning algorithm. Note that we did not say anything yet about the choice of the generalized parameters a and b. This will be clarified in the next section.

IV. Generalized Viviani Curve

In principle, there is a number of ways to construct spherical figure eights, including manual specification and spline interpolation techniques. However, if we look for the solution in the class of elementary functions the choice does not seem to be wide. As a candidate for the figure eight one can use Viviani's curve. This is the curve of intersection of the surfaces of a sphere of radius R and a circular cylinder of radius $R-d$ tangent to the inner surface of the sphere (Figure 5).

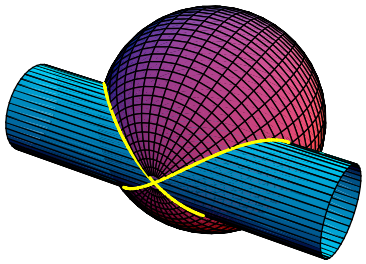

Fig. 5. Formation of the symmetric Viviani curve.

A parameterization of this curve suitable for our problem (setting the tangent plane of the cylinder and the sphere to be the contact plane) can be defined as

$$\bar{\boldsymbol{c}}(\varphi) = \begin{bmatrix} 2\sqrt{d(R-d)}\sin\varphi \\ (d-R)\sin 2\varphi \\ -d+(d-R)\cos 2\varphi \end{bmatrix}, \tag{31}$$

where $\varphi\in[0,2\pi]$. The classical Viviani curve is defined for $d=R/2$. The orthogonal projection of the Viviani curve on the contact plane defines the lemniscate of Gerono, while the stereographic projection defines the lemniscate of Bernoulli. The curve (31) is periodic and consists of two spherical leaves defined by $\varphi\in[0,\pi]$ and $\varphi\in[\pi,2\pi]$.

It should be noted that the curve (31) depends on one parameter d, and its leaves are symmetric. This is not suitable for our motion planning strategy because by tracing the symmetric curve for a fixed number of steps one propels the sphere without changing its orientation. To make the curve (31) asymmetric, one can generalize the Viviani curve and define it as the intersection of a sphere with a cylinder whose axis is inclined and whose radius is variable. Such a cylinder is a cone. The cone is tangent to the inner surface of the sphere as shown in Fig. 6.

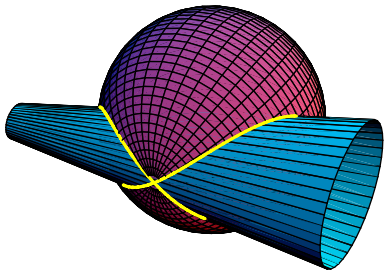

Fig. 6. Formation of the generalized Viviani curve.

Let the axis of the cone be in the OXZ plane. The cone is described by $y^2+(z-z_c)^2=r^2(x)$, where $z_c=r(x)-R$, $r(x)=R-d-x\tan\gamma$ is the variable radius of the cone, and γ is the angle of inclination of the cone's axis. Consider the intersection of the cone with the sphere $x^2+y^2+z^2=R^2$ and define the solution as $y(x)$ and $z(x)$. The z-coordinate of the intersection line is defined as

$$z=\frac{x^2-2R(d+x\tan\gamma)}{2(d+x\tan\gamma)}. \tag{32}$$

while the y-coordinate, $y=\pm\sqrt{R^2-x^2-z^2}$, after some algebra can be represented as

$$y=\pm\sqrt{\frac{x^2(x_{\max}-x)(x-x_{\min})(1+4\tan^2\gamma)}{4(d+x\tan\gamma)^2}}, \tag{33}$$

where

$$x_{\max}=\frac{2(R-2d)\tan\gamma+2\sqrt{d(R-d)+R^2\tan^2\gamma}}{1+4\tan^2\gamma}, \tag{34}$$

$$x_{\min}=\frac{2(R-2d)\tan\gamma-2\sqrt{d(R-d)+R^2\tan^2\gamma}}{1+4\tan^2\gamma}, \tag{35}$$

are the points of, respectively, maximum and minimum, of the x-coordinate. Note that $d+x\tan\gamma\geq 0$ because $r(x)\leq R$, and $r(x)=R$ only in the singular case when the generalized Viviani curve transforms to the circle. Therefore, the representation (33) is defined well.

Next, we need to parameterize $x(\varphi)\in[x_{\min},x_{\max}]$. A "good" parameterization ensures that the derivative $dy/d\varphi=(dy/dx)\,(dx/d\varphi)$ is well defined and does not have singularities at $x=x_{\min}$ and $x=x_{\max}$. To cancel the corresponding radicals in dy/dx, we define $x(\varphi)$ from the differential equation $dx/d\varphi=\sqrt{(x_{\max}-x)(x-x_{\min})}$. The solution satisfying $x(0)=0$ can be written down as follows

$$x(\varphi)=\frac{(x_{\max}+x_{\min})+(x_{\max}-x_{\min})\cos(\varphi-\varepsilon)}{2}, \tag{36}$$

where the angle ε is defined from

$$\cos\varepsilon=-(x_{\max}+x_{\min})/(x_{\max}-x_{\min}). \tag{37}$$

Having defined $x(\varphi)$, by direct calculation we obtain

$$y(\varphi)=\pm\frac{\sqrt{1+4\tan^2\gamma}\,(x_{\max}-x_{\min})\,x(\varphi)\,\sin(\varphi-\varepsilon)}{4(d+x(\varphi)\tan\gamma)}. \tag{38}$$

Thus, the parametric form of the generalized Viviani curve is defined by (36,38,32). If $\gamma=0$ it transforms to the conventional representation (31). The generalized Viviani curve is periodic and consists of two spherical leaves defined by $\varphi\in[0,2\varepsilon]$ and $\varphi\in[2\varepsilon,2\pi]$. Selecting $y(\varphi)$ in (38) with plus sign corresponds to passing the first leave of the curve counterclockwise and the second leave clockwise. Changing the sign to minus changes the direction of passing the curve.

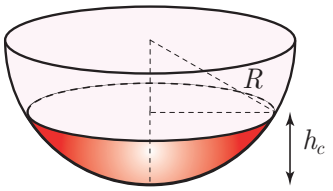

Fig. 7. Admissible contact area.

If the size of the contact area is limited by the height h_c of the admissible spherical cap shown in Figure 7, one sets

$$R-h_c/2<d<R,\quad |\gamma|<\arctan\left(\frac{h_c-2(R-d)}{\sqrt{h_c(2R-h_c)}}\right). \tag{39}$$

To be compatible with the presentation in Section III, one can introduce a more symmetric set of parameters. Let a and b be the radii of the truncated cone at, respectively, the points of maxima and minima of the x-coordinate. Then,

$$a=(R-d)-x_{\max}\tan\gamma,\quad b=(R-d)-x_{\min}\tan\gamma. \tag{40}$$

To satisfy the constraint on the size of the admissible contact area, one sets

$$0<a<h_c/(2R),\quad 0<b<h_c/(2R). \tag{41}$$

It can be shown that the transformation from the parameters a and b to d and γ is defined as

$$d=\frac{(R-a)(R-b)-\sqrt{a(R-a)\,b(R-b)}}{R-(a+b)}, \tag{42}$$

$$\tan\gamma=\pm\frac{1}{2}\left|\frac{\sqrt{a(R-a)}-\sqrt{b(R-b)}}{R-(a+b)}\right|, \tag{43}$$

where one sets plus sign if $b>a$ and minus otherwise. One can also show that in the limiting case $(a+b)\to R$ one has

$$d=R/2,\quad \tan\gamma=\pm\frac{1}{2}\frac{|a-b|}{\sqrt{R^2-(a-b)^2}}. \tag{44}$$

Having constructed the generalized Viviani curve in the form $\bar{\boldsymbol{c}}(a,b,\varphi)$, one can proceeds further and define the non-holonomic shift $h(a,b)$ and the holonomy angle $\eta(a,b)$. It can be deduced from geometric considerations that the non-holonomic shift is symmetric with respect to the parameters a,b, $h(a,b)=h(b,a)$, while the holonomy angle is asymmetric, $\eta(a,b)=-\eta(b,a)$. The values of η and h, normalized with respect to R, are plotted in Figure 8 as functions of a/R and b/R. Inspecting the level curves[2] of

[2]To keep the graph clean, the numerical values of the level sets are not marked in Figure 8. As the structure of the surfaces is not complicated, the change of the level sets can be guessed more or less easily.

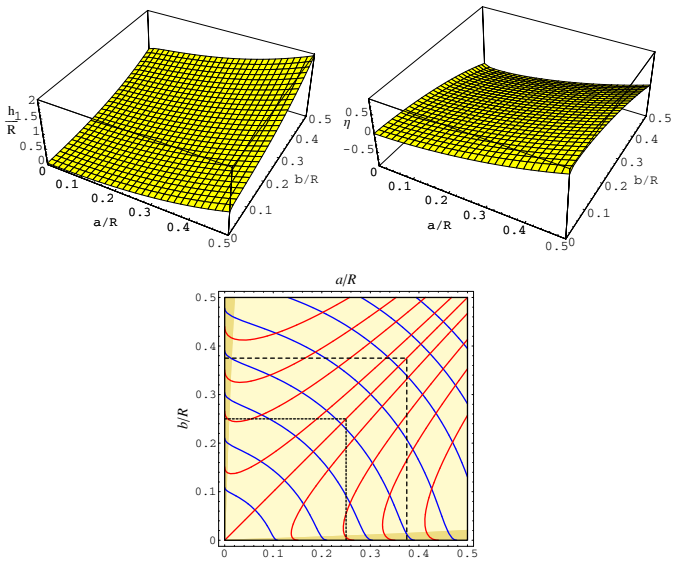

Fig. 8. Normalized non-holonomic shift h/R (top left) and holonomy angle η (top right) as functions of a/R and b/R. Contour lines of h/R (blue) and η (red) are shown in the bottom part for the workspace $h_c/R = 1$, (solid lines), $h_c/R = 3/4$, (dashed lines), and $h_c/R = 1/2$ (dotted lines). The area where the solution of (24,27) is not unique is shown in darker color.

these surfaces, one can see that the solution of the system (24,27), if exists, is unique in a large part of the workspace area. However, if a/R or b/R is relatively small the possible solution may be double-valued (a level line for the surface h/R may cross that for η at two points).

The existence of the solution can be established by inspecting the reachable area of η and h/R when a/R and b/R vary in the admissible intervals corresponding to the assigned ratio h_c/R in (41). The shapes of the reachable area for $h_c/R = 1$, $h_c/R = 3/4$, and $h_c/R = 1/2$ are shown in Figure 9. If the tangent line at the origin of the reachable area is vertical, by setting the number of steps n large enough one can always make the point $\{(h_{\text{des}}/R)\sin(\psi_{\text{des}}/2n)/\sin(\psi_{\text{des}}/2),\ \psi_{\text{des}}/n\}$, $h_{\text{des}} \neq 0$, to lie within the reachable area. Since the analytical expressions for η and h are not available, it is difficult to prove rigorously that the tangent line is vertical at the origin. However, our numerical simulations (zooming by plotting the reachable area for very small ratios h_c/R) show that it appears to hold true.

Let us illustrate the motion planning by the generalized Viviani curve by a simulation example. In the simulation, the initial contact point coordinates are $\boldsymbol{u}_{co} = [0,0]^{\text{T}}(\text{rad})$, $\boldsymbol{u}_{ca} = [0,0]^{\text{T}}(\text{m})$, and the initial relative angle ψ is 0 rad. The desired contact coordinates are set as $\boldsymbol{u}_{co} = [0,0]^{\text{T}}(\text{rad})$, $\boldsymbol{u}_{ca} = [0.2,0.3]^{\text{T}}(\text{m})$, and the desired relative angle ψ is $\pi/6$ rad. The radius R of the hemisphere is 0.2m, and the constraint on the admissible contact area is set as $h_c/R < 1/2$. As can be seen from Figure 9, the minimal number of steps necessary to reach the goal under the specified constraint on the contact area is now $n = 6$. For this number of steps we obtain $a/R \approx 0.2363$, $b/R \approx 0.1822$, and

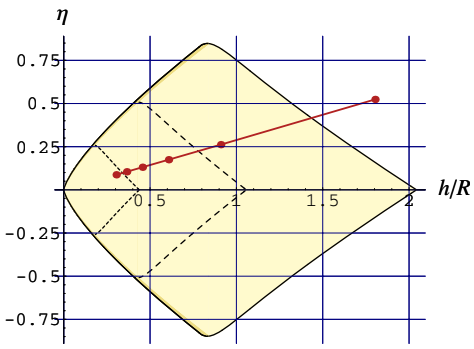

Fig. 9. Reachable area for $h_c/R = 1$, (solid lines), $h_c/R = 3/4$, (dashed lines), and $h_c/R = 1/2$ (dotted lines). The area where the solution of (24,27) is not unique is shown in darker color. The definition of the minimal number of movement steps for the simulation example is shown in brown lines.

$\vartheta \approx -0.1942(\text{rad})$. The evolution of the contact point on the contact plane and on the hemisphere is shown in Figure 10. Note that the whole maneuver is executed by tracing six times the generalized Viviani curve on the hemisphere.

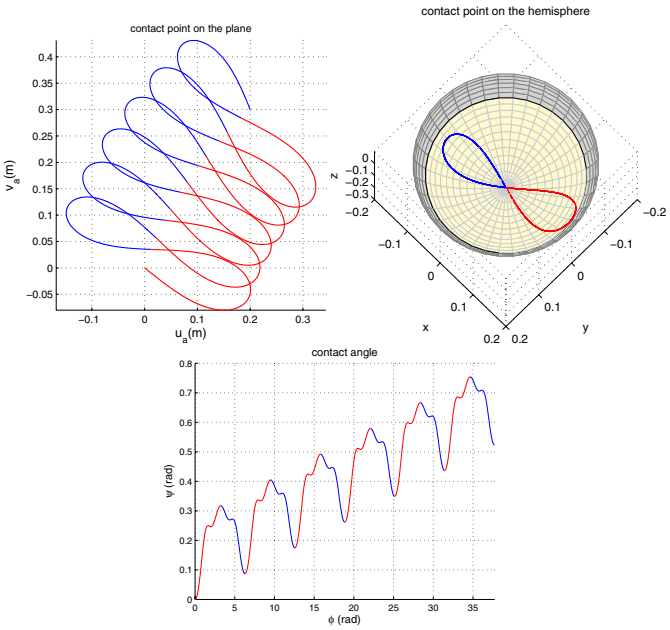

Fig. 10. Trajectory of the contact point on the plane (top left) and on the sphere (top right), and the evolution of the contact angle (bottom). The admissible area on the hemisphere is encircled. The 1st half-step is shown in red, while the 2nd in blue color.

V. Spinning Maneuver

The movement corresponding to $h_{\text{des}} = 0$ and $\psi_{\text{des}} \neq 0$ is called the spinning maneuver [19]. It was discussed, as a part of the general reconfiguration strategy, in [1] but the solution was not completed there. A three-step algorithm for the spinning maneuver, combining two straight line and one circular movements, was proposed in [19].

It should be noted that the algorithm proposed in Section III does not directly work for the spinning maneuver because when $h_{\text{des}} \to 0$ the number of steps $n \to \infty$. Of course, the algorithm can be used as a part of the two-step strategy: *move to an intermediate point and come back with the desired orientation*. But this approach is neither succinct not systematic because the intermediate point can be assigned quite arbitrarily.

A clearer construction of the spinning maneuver in the spirit of Section III (tracing generalized figure eights) can be devised with one simple modification. Note that the movement half-steps in Section III were defined to have different orientation of path tracing, counterclockwise for the first leaf and clockwise for the second. The solution to the spinning maneuver is to keep the orientation the same. If we do so, the contact point on the contact plane would trace closed curves as shown schematically in Figure 11. In the end of tracing the contact coordinates $\boldsymbol{u}_{co}$ and $\boldsymbol{u}_{ca}$ will return to their starting values but the contact angle ψ will change.

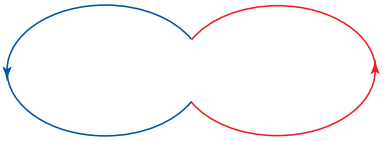

Fig. 11. Trajectory of the contact point on the contact plane for the Viviani curve-based planning of the spinning maneuver.

Since only one coordinate now (the angle ψ) needs to be balanced by the size of the figure eight, it suffices to deal with the symmetric figures. Assume $\psi_{\text{des}} > 0$ (for $\psi_{\text{des}} < 0$ the direction of passing the curves in Figure 11 should be changed to clockwise). Given the number of steps n and the desired orientation ψ_{des}, the size d is defined from $2n\eta(d) = \psi_{\text{des}}$. Given the admissible height of the contact area h_c (and therefore $d_{\min} = R - h_c/2$), the minimal number of steps is clearly $n = \lceil \psi_{\text{des}}/(2\eta(d_{\min})) \rceil$, where $\lceil x \rceil$ rounds the elements of x to the nearest integer more than or equal to x. For the symmetric Viviani curve (31) we can analytically define the area of the spherical leaf and by the Gauss-Bonnet theorem obtain $\eta(d) = 4\left(-\sqrt{\frac{d}{R}(1-\frac{d}{R})} + \arctan(\sqrt{\frac{R}{d}-1})\right)$. It should, however, be noted that in tracing the leaves of the Viviani curve the parameter φ needs to be changed first from 0 to π and then from 2π to π. This results into discontinuity of the higher derivatives at the half-step connection points[3], and in practical implementation these points should be passed with zero instantaneous velocity [18].

Let us now show how to construct C^∞ trajectories for the spinning maneuver. For this purpose, we resort to the Cassini curve whose different shapes are shown in Figure 12. The shapes are defined by two parameters, a and b. Place the start point at the origin and select the positive (counterclockwise) direction of passing the curve. The coordinates of the contact point on the contact plane, parameterized by the Cassini curve, are defined as

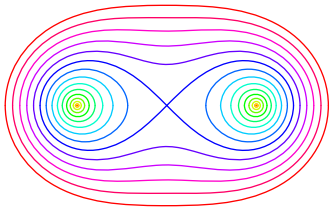

Fig. 12. The shapes of the Cassini curve.

$$\boldsymbol{u}_{ca}(\varphi) = \begin{bmatrix} a\sin\varphi\sqrt{\sqrt{(b/a)^4 - \sin^2 2\varphi} - \cos 2\varphi} \\ d - a\cos\varphi\sqrt{\sqrt{(b/a)^4 - \sin^2 2\varphi} - \cos 2\varphi} \end{bmatrix}, \tag{45}$$

where $d = \sqrt{b^2 - a^2}$ and $\varphi \in [0, 2\pi]$. This parameterization is valid only for $b > a$, which is what we need[4]. In the limiting case $b \to \infty$ the curve becomes the circle. Note that for our purpose the curve must be concave. Otherwise, tracing the curve would not produce figure eights on the sphere. This results to the restriction $b/a < \sqrt{2}$.

The remaining is similar to what has been presented in Section III, only now we deal with the differential equations (6-8). Integrating the system (6-8) numerically for one step of movement ($\varphi \in [0, 2\pi]$) with zero initial conditions, one defines, using the spherical distance, the nonholonomic shift on the sphere $h(a,b) \triangleq R\arccos\left(\cos(u_o(2\pi))\cos(u_o(2\pi))\right)$ and the holonomy angle $\eta(a,b) \triangleq \psi(2\pi)$. The parameters a and b can then be obtained by solving the system $h(a,b) = 0$, $\eta(a,b) = \psi_{\text{des}}/n$. As the first equation here constrains the choice of the parameters a and b, the function η defines a three-dimensional curve. This curve and its projections on the coordinate planes are shown in Figure 13.

Note that for the solution $u_o(\varphi), v_o(\varphi)$ to be admissible, the height of the resulting spherical curve should be limited by the height of the admissible contact area shown in Figure 7. From considerations of symmetry the highest points on the spherical curve correspond to $\varphi = \pi/2 + k\pi$, $k \in \mathbb{Z}$, in the parameterization (45), and the admissibility condition can be defined as $1 - \cos u_o(\pi/2)\cos v_o(\pi/2) < h_c/R$. If, for a given n, it is not satisfied the number of steps in solving the system $h(a,b) = 0$, $\eta(a,b) = \psi_{\text{des}}/n$ must be increased.

Consider, for the illustration, a simulation example where $\psi_{\text{des}} = \pi$, i.e. the hemisphere needs to be completely reoriented. As before, set $R = 0.2$m and $h_c/R = 1/2$. If there is no constraint on the admissible contact area it is possible to complete the maneuver in one step (with $h_c/R \approx 1.1628$). To satisfy the constraint $h_c/R = 1/2$ we sequentially increase n and find the minimal number of movement steps $n = 4$ (see Figure 13). For this number of steps we obtain $a/R \approx 0.6511$, $b/R \approx 0.6593$ from solving the system $h(a,b) = 0$, $\eta(a,b) = \psi_{\text{des}}/n$. The simulation

[3]Also note that to guarantee that the curve on the contact plane is closed, the angle ϑ at the connection points needs to be changed discontinuously.

[4]It follows from the implicit equation of the Cassini curve that when $b = a$ it is transformed to the lemniscate of Bernulli, and when $b < a$ it splits into two ovals [20]. These cases are not relevant to our purpose.

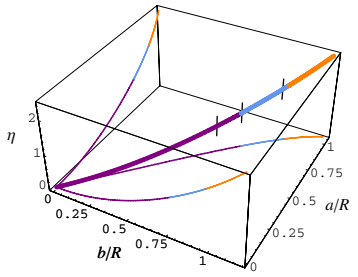

Fig. 13. Phase shift η and its projections on the coordinate axes. The part corresponding to $h_c/R \in [0, 1/2]$ in shown in purple, $h_c/R \in [1/2, 3/4]$ in blue, and $h_c/R \in [3/4, 1]$ in orange. The points corresponding to $n = 2, 3, 4$ in the simulation example are marked by vertical bars.

results for the evolution of the contact point on the contact plane and on the hemisphere are shown in Figure 14.

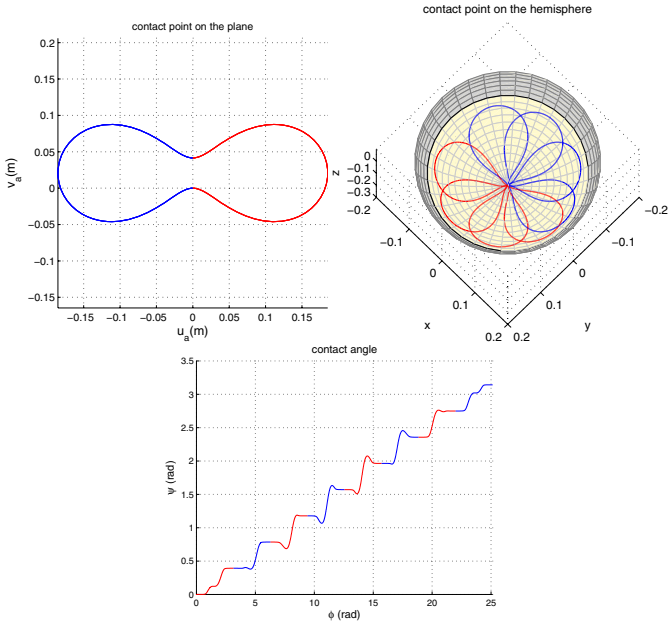

Fig. 14. Trajectory of the contact point on the plane (top left) and on the sphere (top right), and the evolution of the contact angle (bottom).The admissible area on the hemisphere is encircled. The 1st half-step is shown in red, while the 2nd in blue color.

VI. Conclusions

The motion planning for a rolling system with limited contact area has been discussed in this paper. Under the constraints imposed on the size of the contact area, the construction of motion for this task can be regarded as a hybrid problem of parallel parking in a finite number of movement steps. A motion planning algorithm, realizing the movement steps by tracing smooth figure eights on the hemisphere, has been proposed. To generate asymmetric figure eights, a generalization of the Viviani curve is proposed. An exceptional case of the algorithm, corresponding to the spinning maneuver, is constructed with the use of the Cassini curve. The convergence of the algorithm has been analyzed, and the computational feasibility has been verified under simulation. The algorithm can be useful when generating C^∞ trajectories is required. However, compare to the conventional (triangles or circle-based) algorithms, it comes with the price of heavier (but still feasible) computations. These considerations should be taken into account when designing motion planner for specific applications.

References

[1] Z. Li and J. Canny, "Motion of two rigid bodies with rolling constraint," *IEEE Trans. on Robotics and Automation*, vol. 6, no. 1, pp. 62–72, 1990.

[2] A. Bicchi, A. Marigo, and D. Prattichizzo, "Robotic dexterity via nonholonomy," in *Control Problems in Robotics and Automation*, ser. LNCIS 230, B. Siciliano and K. Valavanis, Eds. Berlin Heidelberg, Germany: Springer Verlag, 1997, pp. 35–49.

[3] H. Date, M. Sampei, M. Ishikawa, and M. Koga, "Simultaneous control of position and orientation for ball-plate manipulation problem based on time-state control form," *IEEE Transactions on Robotics*, vol. 20, no. 3, pp. 465–480, June 2004.

[4] T. Das and Mukherjee, "Exponential stabilization of the rolling sphere: An intractable nonholonomic system," *Automatica*, vol. 40, no. 11, pp. 1877–1889, November 2004.

[5] G. Oriolo and M. Vendittelli, "A framework for the stabilization of general nonholonomic systems with an application to the plate-ball mechanism," *IEEE Transactions on Robotics*, vol. 21, no. 2, pp. 162–175, 2005.

[6] T. Das and Mukherjee, "Reconfiguration of a rolling sphere: A problem in evolute-involute geometry," *ASME Journal of Applied Mechanics*, vol. 73, no. 4, pp. 590–597, July 2006.

[7] A. Arthurs and G. Walsh, "On Hammersley's minimum problem for a rolling sphere," *Mathematical Proceedings of the Cambridge Philosophical Society*, vol. 99, no. 3, pp. 529–534, 1986.

[8] R. Brockett and L. Dai, "Non-holonomic kinematics and the role of elliptic functions in constructive controllability," in *Nonholonomic Motion Planning*, Z. Li and J. Canny, Eds. Boston: Kluwer Academic Publishers, 1992, pp. 1–21.

[9] V. Jurdjevic, "The geometry of the plate-ball problem," *Archive for Rational Mechanics and Analysis*, vol. 124, no. 4, pp. 305–328, December 1993.

[10] M. Levy, "Geometric phases in the motion of rigid bodies," *Archive for Rational Mechanics and Analysis*, vol. 122, no. 3, pp. 213–229, September 1993.

[11] R. Murray, Z. Li, and S. Sastry, *A Mathematical Introduction to Robotic Manipulation*. Boca Raton: CRC Press, 1994.

[12] R. Mukherjee, M. Minor, and J. Pukrushpan, "Motion planning for a spherical mobile robot: Revisiting the classical ball-plate problem," *ASME Journal of Dynamic Systems, Measurement and Control*, vol. 124, no. 4, pp. 502–511, 2002.

[13] A. Marigo and A. Bicchi, "Rolling bodies with regular surface: Controllability theory and applications," *IEEE Trans. on Automatic Control*, vol. 45, no. 9, pp. 1586–1599, September 2000.

[14] K. Harada, T. Kawashima, and M. Kaneko, "Rolling based manipulation under neighborhood equilibrium," *The International Journal of Robotics Research*, vol. 21, no. 5-6, pp. 463–474, 2002.

[15] A. Bicchi and A. Marigo, "Dexterous grippers: Putting nonholonomy to work for fine manipulation," *The International Journal of Robotics Research*, vol. 21, no. 5-6, pp. 427–442, May-June 2002.

[16] S. Sekhavat and J. Laumond, "Topological properties for collision free nonholonomic motion planning: The case of sinusoidal inputs for chained form systems," *IEEE Transactions on Robotics and Automation*, vol. 14, no. 5, pp. 671–680, 1998.

[17] A. Nakashima, K. Nagase, and Y. Hayakawa, "Control of a sphere rolling on a plane with constrained rolling motion," in *Proc. IEEE Int. Conference on Decision and Control*, vol. 3, Seville, Spain, December 12–25 2005, pp. 1445–1452.

[18] M. Svinin and S. Hosoe, "On motion planning for ball-plate systems with limited contact area," in *Proc. IEEE Int. Conference on Robotics and Automation*, Rome, Italy, April 10-14 2007, pp. 1820–1825.

[19] G. Oriolo, M. Vendittelli, A. Marigo, and A. Bicchi, "From nominal to robust planning: The plate-ball manipulation system," in *Proc. IEEE Int. Conference on Robotics and Automation*, vol. 4, Taipei, Taiwan, September 14–19 2003, pp. 3175–3180.

[20] A. Gray, *Modern Differential Geometry of Curves and Surfaces with Mathematica*, 2nd ed. Boca Raton: CRC Press, 1998.